Advanced Nanoscale Elastic Property Measurement by Contact-Resonance Atomic Force Microscopy

G. Stan and R. F. Cook

Nanomechanical Properties Group, National Institute of Standards and Technology, Gaithersburg, MD, USA, gheorghe.stan@nist.gov, robert.cook@nist.gov

ABSTRACT

In atomic force microscopy (AFM)-based techniques, material information (topography, mechanical, electrical, magnetic, etc.) is retrieved from the nanoscale interaction between the AFM tip and the material probed. As the size of the apex of the AFM tip is comparable with the size of the investigated structures, it is very important to recognize the tip contribution to the quantities measured. In particular, this is necessary when nanoscale elastic properties are probed by contact-resonance AFM (CR-AFM), in which case, the tip contribution needs to be considered in both the topographical and contact mechanical responses. By combining topography and mechanical response, an advanced characterization of non-flat nanoscale structures by CR-AFM has been accomplished. Two major applications will be discussed here: (1) self-correlation of the topography image and contact stiffness map for a granular Au film and (2) point measurements across oxidized Si nanowires.

Keywords: nanoscale elastic modulus, contact resonance, atomic force microscopy, nanowires

1 INTRODUCTION

Invented two decades ago [1], atomic force microscopy (AFM) now provides simple and direct access to nanoscale investigations of material surfaces. Besides the common topography mapping, over the years innovative AFM modes have advanced and differentiated AFM nanoscale characterization by exploiting the sensitive detection of probe-sample interactions: In the class of dynamic AFM modes, contact resonance atomic force microscopy (CR-AFM) [2] [3] distinguishes itself as a sensitive technique for quantitative measurements of the elastic responses of materials at the nanoscale. CR-AFM has been used successfully to measure the elastic properties of a large variety of materials and structures: piezoelectric ceramics [4], metal films [5], diamond-like carbon films [6], glass-fiber-polymer matrix composites [7], clay minerals [8], polycrystalline materials [9], and nanostructures (nanobelts [10], nanowires (NWs) [11], and nanotubes [12]). In the past few years, we have improved and developed the capabilities of CR-AFM in various ways: established clear criteria for assessing the precision and accuracy in CR-AFM measurements [13], introduced a load-dependent CR-AFM protocol [14] suitable for elastic modulus measurements on compliant materials, and tested the suitability of CR-AFM measurements on various materials with elastic moduli in the range of few GPa to hundreds of GPa. In the new load-dependent CR-AFM approach, the deflection and resonance frequency shift of the AFM cantilever-probe are recorded simultaneously as the probe is gradually brought in and out of contact. Another valuable CR-AFM application has been the mapping of elastic properties at the nanoscale of granular nanocrystalline surfaces [15] and microstructures [16]. By combining the CR-AFM point measurements with AFM scanning capability, the elastic modulus was mapped with better than 10 nm spatial resolution. To determine the elastic modulus from CR-AFM measurements on non-flat surfaces, both topography and contact stiffness maps were self-consistently correlated. We have also extended CR-AFM applicability to quantitative elastic modulus measurements on various one-dimensional nanostructures (NWs [11] [17] and nanotubes [12]). From such CR-AFM measurements, not only were the mechanical properties of nanostructures probed but also intriguing characteristics of the nanoscale structure-mechanical properties relationship were revealed. In the case of ZnO NWs [11] and Te NWs [17], the elastic moduli were found to be strongly size dependent for diameters less than 100 nm. From recent CR-AFM measurements on oxidized Si NWs [18], the effect of the compressive stress at the Si-SiO_2 interface was revealed in the diameter dependence of the elastic moduli of these NWs. In this work we will review some advances in using the topographical information to retrieve correctly the local elastic response of nanostructures probed by CR-AFM. This is necessary when non-flat surfaces are imaged by CR-AFM and the local nanoscale elastic response has to be amended for the continuous change in the contact geometry during scanning. The example here will be for a granular Au surface, with local changes in the contact spring couplings imposed by the topographical variations. A precise determination of the size of the structure measured is critical also in establishing the correct contact geometry in CR-AFM point-measurements across one-dimensional structures; as an example, the CR-AFM

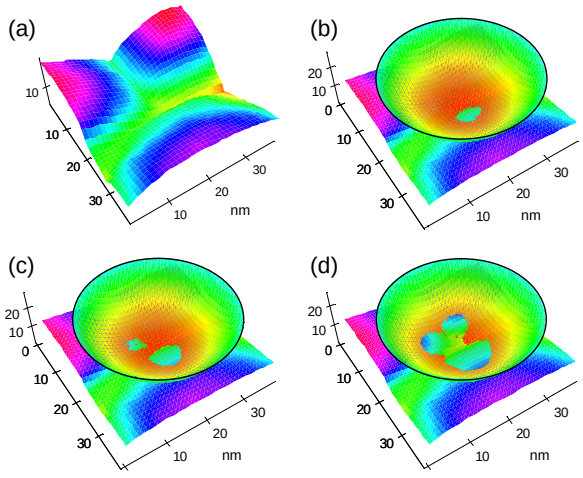

Figure 1: Progressive contact intersection between the apex of the AFM tip of radius 34.4 nm and a triple junction of a granular Au surface as the applied load was increased from (a) 0, to (b) 100 nN, (c) 250 nN, and (d) 350 nN, respectively.

analysis will be shown here for elastic modulus measurements of oxidized Si NWs.

2 CR-AFM Application To Image Nanoscale-Rough Surfaces

In CR-AFM, a small-amplitude oscillation that vibrates the tip-sample contact excites acoustic waves in the sample and the resonance state of the clamped-coupled cantilever system changes accordingly. The elastic response of the material is retrieved then from the variation experienced by the resonance frequency of the AFM cantilever. Besides the dynamical analysis that converts directly the measured resonance frequencies into the tip-sample contact stiffness, the final step consists of extracting the elastic modulus of the sample from the calculated contact stiffness through a contact mechanics model that adequately describes the contact formed between tip and sample. On non-flat surface topographies, variations in the contact geometry need to be known a priori and incorporated into the contact model used. In the case of a complex contact geometry it could be relevant for not only the normal component but also the lateral component of the tip-sample coupling. Ultimately, the normal and lateral contact couplings alter the dynamics of the cantilever and their effect is observed in additional changes of the contact resonance frequencies of the cantilever. Detail reviews of CR-AFM operation, measurement analysis, and applications can be found in Refs. [19], [20], and [21].

On nanoscale-rough surfaces, the contact geometry changes not only in size by also through the number of contacts established between the scanning tip and adjacent contacted material, varying from single-asperity contact (SAC) to multiple-asperity contact (MAC) [15]. Such an example is shown in Fig. 1 where the apex of the AFM tip was brought gradually into contact with the intergrain region formed between three adjacent Au grains. As the applied load was increased progressively from 0 to 350 nN, the contact evolved from SAC to MAC. The contacted grains act as individual springs with the load distributed between their summits. In such cases of complicated contact geometries, the actual topography, free of tip artifacts, needs to be used for a correct interpretation of the contact mechanics contained in the CR-AFM measurements.

Two scan images, contact resonance frequency and topography (see Figs. 2a and 2b), were acquired over the same area of about 600 nm^2 of the granular Au film. The contact resonance frequency map (Fig. 2b) was reconstructed from the frequency spectra acquired at every point in the scan (125 x 125 pixels) by a lock-in amplifier detection technique [15]. Subsequently, the scanning tunneling microscopy (STM) mode of the same AFM used for CR-AFM was chosen to re-scan the same investigated area and provide high-resolution details of the scanned topographical features (Fig. 2a). A very good feature correspondence can be observed between the two images and they can be self-consistently correlated. Using the information from STM and CR-AFM maps, at every location in the scan, the contact reconstruction is processed for the tip radius and applied load used in CR-AFM scan. Thus, the tip and surface were simulated to come into contact by gradually increasing the load until it reached the value of the applied load. Once the setpoint was reached, the contact geometry was observed to be either from a SAC or MAC. We point out that this is an advanced approach in tip-sample contact reconstruction as it includes the local elastic deformation of the tip and surface.

With the self-consistent consideration of the elastic properties of the contacted surface, the maps for the contact area and elastic modulus are obtained (see Figs. 2c and 2d). Good correlations and intriguing details are observed between the four maps. Nominally, a slight reduction in the elastic modulus in the intergrain regions is expected as a result of the orientation mismatch between adjacent grains. On contrary, in Fig. 2b, the contact resonance frequency is observed to increase in the intergrains regions. The explanation is that, as can be seen in Fig. 2c, the contact area increases in the intergrain regions due to MAC formation. This in turn determines an increase in the contact resonance frequency, but its proper consideration provide the correct calculation for the elastic modulus. Indeed, the elastic modulus (Fig. 2d) decreases consistently in the intergrain regions. In addition to that, small variations in the contact area

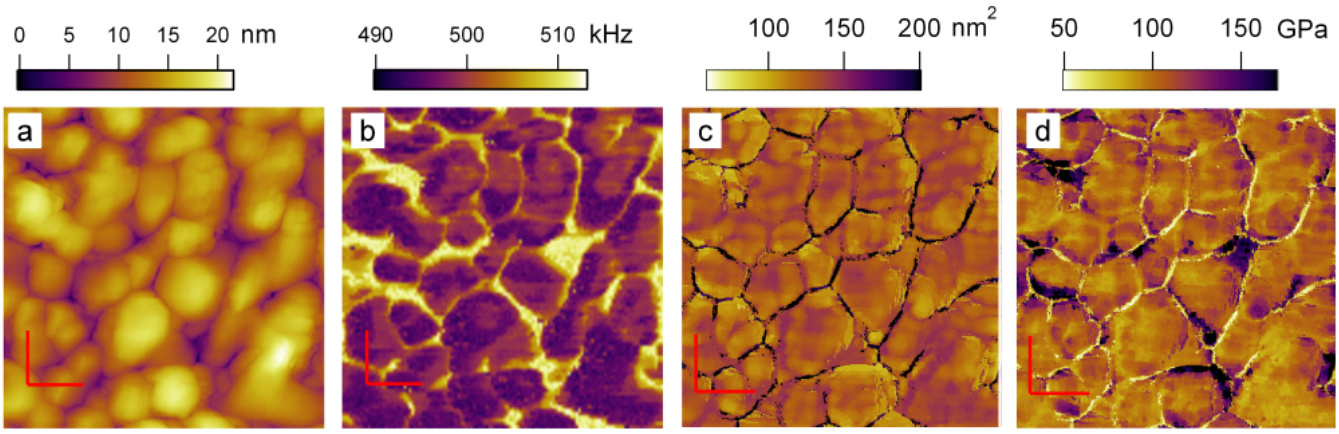

Figure 2: (a) Topography and (b) contact-resonance frequency map, acquired over the same area of a granular Au film, are self-consistent correlated to calculate (c) the contact area and (d) elastic modulus maps. The horizontal and vertical scale bars are 100 nm in every image.

and elastic modulus are also observed within grain regions. As can be seen in Fig. 2d, there are still unresolved regions (grain boundaries with sharp ripples) where the contact geometry is not described properly by the Hertzian contact model used; in such cases finite element analysis could be a viable alternative.

3 CR-AFM Application To One-Dimensional Structures

The measurement of mechanical properties of one-dimensional structures is important both for understanding the material-structure relationship at the nanoscale and practical applications. Among the multitude of nanostructures, Si NWs have distinctively remarkable electrical, mechanical, optical, and thermoelectric properties that can be exploited in building-blocks of various nanodevices. From CR-AFM measurements of the elastic modulus of as-grown and oxidized Si NWs, we have found that the mechanical properties of oxidized Si NWs can be slightly tuned by the stress developed at the Si-SiO_2 interface during the oxidation process.

CR-AFM measurements were performed on three types of Si NWs: as-grown Si NWs, Si NWs oxidized at 900 °C for 5 min, and Si NWs oxidized at 1000 °C for 5 min. As in the case of the granular topography analyzed above, the correct consideration of the contact geometry is necessary in converting the measured contact resonance frequencies into the elastic modulus. The measurements, as shown in Fig. 3a, were made along a path perpendicular to the NW probed, starting on the substrate, passing over the NW, and ending on the substrate. The contact geometry during these measurements changes from sphere-to-flat on the substrate to sphere-on-cylinder on the NW, with the normal applied force varying across the NW. The parameters needed to resolve these contact geometries were extracted from regular AFM scans encompassing the NW. At every location, both the deflection of the cantilever and its resonance frequency were recorded as the tip was brought gradually in and out of contact (refer to Fig. 3a). The measured signals were combined to determine the force dependence of the contact stiffness over the range of the applied forces (less than 50 nN). The Hertzian contact mechanics model was then used to fit the load-dependent contact stiffness measured on each NW and determined the radial elastic moduli of the NWs probed.

In the investigated range of NW radii, between 15 nm and 55 nm, for as-grown Si NWs (orientated along $< 112 >$ direction) and fully oxidized Si NWs (those oxidized at 1000 °C for 5 min) no significant variations were observed in their elastic modulus as a function of radius. Their measured elastic moduli, around 160 GPa for as-grown Si NWs and 75 GPa for fully oxidized Si NWs (dotted lines in Fig. 3b), are close to the known values of bulk Si and SiO_2, respectively. Contrary to that, a clear radius dependence was observed for the elastic modulus of Si NWs oxidized at 900 °C for 5 min. With the exact knowledge of the Si core-SiO_2 structure geometry, the elastic modulus of these NWs can be calculated from a core-shell model [11]. However, a good data fit [18] was obtained with a modified core-shell model that includes the contribution from the mechanically modified Si-SiO_2 interface (refer to the gray curve in Fig. 3b with the interface stress specified on the graph). This interface stress originates from the difference between the volumes of consumed Si and newly formed SiO2. As the oxide is progressively formed at the Si-SiO_2 interface, it is pushed outwards and a radial compressive stress is developed at the interface and decays towards the free surface of the oxide [22]. From the radius dependence

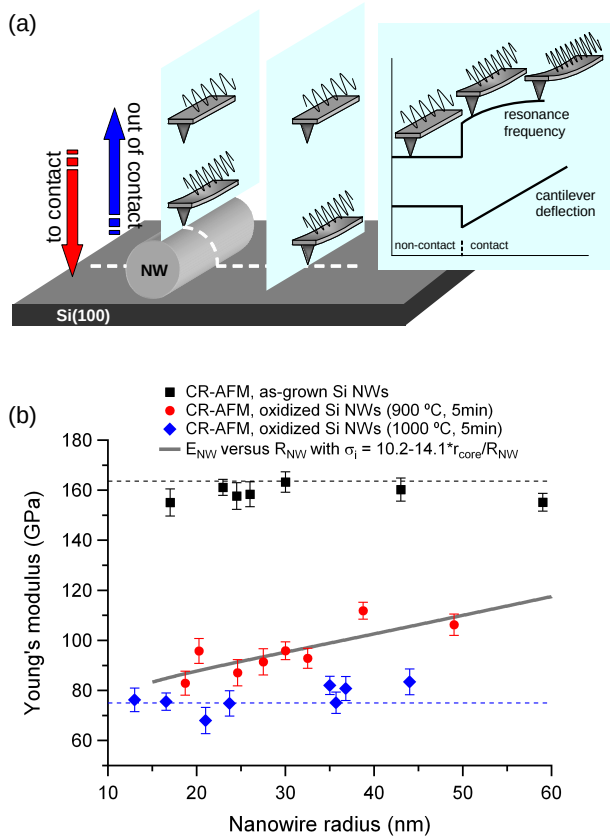

Figure 3: (a) Load-dependent CR-AFM measurements were performed along a direction perpendicular to an investigated NW. At points along this path (dotted trace), on the substrate as well as over the NW, the resonance frequency and deflection of the cantilever were both recorded as the probe was gradually brought in and out of contact with the sample tested. The resonance frequency changes as a function of material probed (substrate or NW), contact geometry, and applied force. (b) Radius dependence of the elastic modulus of as-grown Si NWs, Si NWs oxidized at 900 °C for 5 min, and Si NWs at 1000 °C for 5 min.

of the elastic modulus determined in our CR-AFM measurements, the interface stress is predicted to increase with the decrease in the NW radius and this is because, as the NW radius increases, the oxide shell thickness becomes thicker and a less deformed oxide is accommodated.

In this application, from CR-AFM measurements performed on the outer surface of oxidized Si NWs, we were able to probed the effect of the buried Si-SiO_2 interface on the elastic modulus of these nanostructures. This demonstrates the application of using CR-AFM in probing the mechanical properties of subsurface interfaces.

REFERENCES

[1] G. Binning, C. F. Quate, and C. Gerber, Phys. Rev. Lett. 56, 930, 1986.

[2] U. Rabe, K. Janser, and W. Arnold, Rev. Sci. Instrum., 67, 3281, 1996.

[3] K. Yamanaka and S. Nakano, Jpn. J. Appl. Phys., 35, 3787, 1996.

[4] U. Rabe, M. Kopycinska, S. Hirsekorn, J. Munoz Saldana, G. A. Schneider, W. Arnold, J. Phys. D: Appl. Phys, 35, 2621 (2002).

[5] M. Kopycinska-Muller, R. H. Geiss, J. Muller, D. C. Hurley, Nanotechnology, 16, 703, 2005.

[6] D. Passeri, A. Bettucci, M. Germano, M. Rossi, A. Alippi, Appl. Phys. Lett., 88, 121910, 2006.

[7] D. C. Hurley, M. Kopycinska-Muller, A. B. Kos, R. H. Geiss, Adv. Eng. Mater., 7, 713, 2005.

[8] M. Prasad, M. Kopycinska, U. Rabe, W. Arnold, Geophys. Res. Lett., 29, 31, 2002.

[9] A. Kumar, U. Rabe, S. Hirsekorn, W. Arnold, Appl. Phys. Lett., 92, 183106, 2008.

[10] Y. G. Zheng, R. E. Geer, K. Dovidenko, M. Kopycinska-Muller, D. C. Hurley, J. Appl. Phys., 100, 124308, 2006.

[11] G. Stan, C. V. Ciobanu, P. M. Parthangal, and R. F. Cook, Nano Lett., 7, 3691, 2007.

[12] G. Stan, C. V. Ciobanu, T. P. Thayer, G. T. Wang, J. R. Creighton, K. P. Purushotham, L. A. Bendersky, and R. F. Cook, Nanotechnology, 20, 035706, 2009.

[13] G. Stan and W. Price, Rev. Sci. Instrum., 77, 103707, 2006.

[14] G. Stan, S. W. King, and R. F. Cook, J. Mater. Res., 24, 2960, 2009.

[15] G. Stan and R. F. Cook, Nanotechnology, 19, 235701, 2008.

[16] G. Stan, S. Krylyuk, A. V. Davydov, M. D. Vaudin, L. A. Bendersky, and R. F. Cook, Ultramicroscopy, 109, 929, 2009.

[17] G. Stan, S. Krylyuk, A. V. Davydov, M. Vaudin, L. A. Bendersky, and R. F. Cook, Appl. Phys. Lett., 92, 241908, 2008.

[18] G. Stan, S. Krylyuk, A. V. Davydov, and R. F. Cook, submitted, 2010.

[19] U. Rabe, in "Applied Scanning Probe Methods II", pp 37-90, ed. B. Bhushan and H. Fuchs, Berlin, Springer, 2006.

[20] D. C. Hurley, in "Applied Scanning Probe Methods IX", pp. 97-138, ed. B. Bhushan and H. Fuchs, Berlin, Springer, 2009.

[21] G. Stan and R. F. Cook, in "Scanning Probe Microscopy in Nanoscience and Nanotechnology", pp. 571-611, ed. B. Bhushan, Berlin, Springer, 2010.

[22] D. B. Kao, J. P. McVittie, W. D. Nix, and K. Saraswat, IEEE Trans. Electron. Devices, ED-35, 25, 1988.